한국소음진동공학회 2003년도 추계학술대회논문집, pp. 424~430.

PZT를 이용한 초소형 광 픽업 엑츄에이터의 슬라이딩 모드 제어

Sliding mode control of small form factor optical pick-up actuator using PZT

이 우 철* · 정 동 하** · 박 태 욱*** · 박 노 철*** · 양 현 석****

Woo-Chul Lee, Dong-Ha Jung, Tae-Wook Park, No-Cheol Park, Hyun-Seok Yang

Key Words : Dual-stage Actuator; Swing-arm; Sliding mode control; Bimorph PZT; Optical Disk Drive.

ABSTRACT

This paper proposes a swing-arm type dual-stage actuator, which consists of a PZT actuator for fine motion and a VCM(Voice Coil Motor) for coarse motion, for SFF ODD(Small Form Factor Optical Disk Drive), in order to achieve fast access speed and precise track following control. We focus our attention on the design and control of the PZT actuator, because there have been a lot of previous researches related to the VCM and dual-stage actuators. Due to the dual cantilever structure, the PZT actuator can generate precise translational tracking motion at its tip where optical pickup is attached at, and the effect of hysteric behavior of the PZT element is reduced. The dynamic model of the PZT actuator is derived by using the Hamilton's principle, and verified by comparing with the experimental frequency response. The sliding mode control is designed in order to be robust against modeling uncertainties. Simulations and experimental results confirm the effectiveness of the suggested control scheme.

1. 서 론

Recent developments in portable consumer devices call for storage systems solutions using compact drive units and cheap storage media. HDDs(Hard disk drives) and solid state storages such as Compact Flash and Smart Media are now being incorporated in small sized mobile devices such as PDAs, camcorders and digital photo cameras. However, the price per unit capacity of those storage devices is not cheap and there is no read-only media for mass distribution of data in them. On the other hand, the media of the ODD(Optical Disk Drive) are very cheap and it is easy to manufacture very cheaply the replicated read-only media. In spite of these advantages in ODD technologies, the small form factor ODD for mobile devices has not well developed.

In the present conventional ODD, a worm gear or a rack-and-pinion is used as the coarse motion mechanism for moving the pickup unit. The power transmission ratio of these mechanisms is good, but the access speed of the drive using them is much slower than that of HDDs and they are apt to generate noise and unnecessary vibration. Furthermore, in fine motion actuator, the objective lens is supported by a 4-wire suspension spring, and thus there may exist coupling modes between tracking and focusing direction. These coupling modes can lead to the misalignment of the optical axes. In addition, conventional actuator is difficult to be fabricated in small size because it consists of a number of components. Thus, it is necessary to develop a new actuator mechanism for small-sized, high density, and fast access ODD.

On the other hand, HDDs use the swing arm type VCM(Voice Coil Motor) actuator that is suitable for fast access and small form factor. As the track density of HDDs has increased, numerous works on the development of the dual-stage actuator that consists of VCM and PZT and effective control algorithms are available.[1,2,3]

In this study, we propose a swing arm type dual-stage actuator using a conventional VCM as the coarse motion actuator and a PZT actuator as the fine motion actuator. Most of developed technologies for the dual-stage actuator of HDDs can be applied to the proposed actuator. However, as shown in the previous study conducted by Cho et. al.[1], the structure of the PZT actuator is completely different to those of the dual-stage actuator for HDDs. Therefore, there is need to study the PZT actuator in order to analysis its dynamic characteristics and develop efficient controller for it.

In previous study of the proposed actuator[1], we can show that it is suitable for fast seeking motion and residual vibration in fine actuator can be successfully suppressed. However, there are need to model the fine actuator precisely and develop robust track following controller for the PZT actuator. We focus our attention on design and control of the PZT actuator, because there have been a lot of previous researches related to the VCM and dual actuators.

The paper organized as follows: In section 2,construction of proposed dual-stage actuator and

* 연세대학교 대학원 기계공학과
E-mail : woochul7@hanmail.net
Tel : (02) 2123-2824, Fax : (02) 364-6769

** 삼성전자 OMS 사업부

*** 연세대학교 정보저장공학과

**** 연세대학교 기계공학과

moving mechanism of PZT actuator are described. In section 3, dynamic model of PZT actuator is derived by using Hamilton's principle and compared with frequency response and FEM analysis. In section 4, control model of PZT actuator is formulated by considering hysteric behavior of PZT and parameter variations such as natural frequency and damping ratio. And sliding mode controller known to be robust to model uncertainty is designed to achieve precise track following control. In section 5, linear observer to get observed state vector is designed. In section 6, sliding mode controller combined with linear observer is experimentally implemented. Finally, in section 7, conclusions are provided.

2. Dual-stage actuator

The proposed dual-stage actuator consists of a rotary VCM and a PZT actuator as shown in Fig.1. The dual-stage actuator is charged with the motion of tracking direction, and it holds optical head that consists of optical pickup and focusing actuator. In this study, the optical head is replaced by equivalent dummy mass of 0.6g. The VCM, the coarse motion actuator, can move rapidly over large number of tracks and the PZT actuator, the fine motion actuator, can implement high precise track following motion. Therefore, the proposed dual-stage actuator can achieve fast access speed, high bandwidth and high precise track following.

The structure of PZT actuator has several advantages over other types of PZT actuators. For example, it can minimize the effect of the hysteric behavior in PZT elements, and generate precise translational tracking motion at its tip where optical pickup is attached at. And it is easy to make in small size compared to the conventional sled type actuator. Due to the ferroelectric nature, PZT shows hysteresis effect when voltage is applied. However, if a pair of PZT actuators is arranged in parallel and voltages are applied such that it deflects in "S" shape with tension-compression as shown in Fig.2, the upper PZTs and the lower PZTs move in opposite direction in hysteresis loop. Thus, the effect of hysteric behavior can be reduced at the end of the PZT actuator.

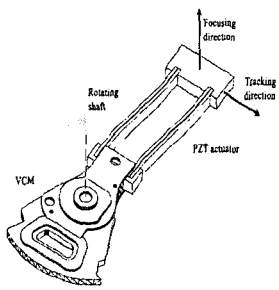

Fig. 1. Proposed dual stage actuator

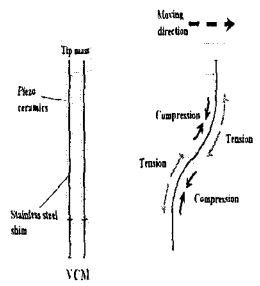

Fig. 2. "S"shape moving mechanism of PZT actuator

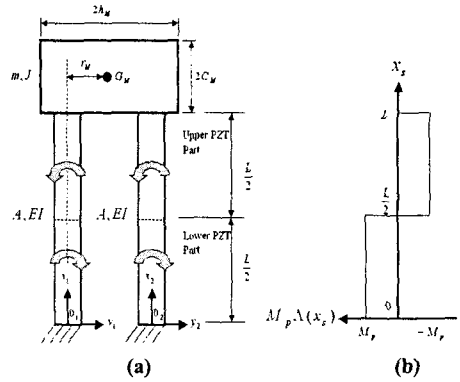

Fig. 3. (a) Simple model for PZT actuator. (b) Bending moment diagram.

3. Dynamic model of PZT actuator

PZT actuator can be considered as a system consisting of a pair of identical elastic cantilevers and carrying a rigid platform of mass fixed at the tip. The geometry and coordinates are shown in Fig. 3(a). The left $(s = 1)$ and right $(s = 2)$ flexible beams are assumed to be Bernoulli-Euler beams with mass per length ρA, effective bending stiffness EI, length L, and connected with tip mass m $(s = 3)$. Shear and rotational inertia effects are assumed to be negligible. To formulate the equations of motion of this system, let the $o_1x_1y_1$ and the $o_2x_2y_2$ axes be inertial frames. Kinetic energy and potential energy of PZT actuator take the form as Eq. (1). $u_s(x_s,t)$ and $w_s(x_s,t)$ are displacements of longitudinal and translational directions, respectively, and $s = 1$ and 2 are described in $o_1x_1y_1$ and $o_2x_2y_2$, respectively.

$$T_s = \frac{1}{2}\int_0^L \rho A\left[\dot{u}_s^2 + \dot{w}_s^2\right]dx_s,$$
$$V_s = \frac{1}{2}\int_0^L \left[EAu_s'^2 + EIw_s''^2\right]dx_s, \quad (s=1,2), \tag{1}$$
$$T_3 = \frac{1}{2}m\left(\dot{u}_1^2(L,t)+\dot{w}_1^2(L,t)\right)+\frac{1}{2}J\dot{w}_1'^2(L,t)+m\left(C_M\dot{w}_1'(L,t)\dot{w}_1(L,t)-r_M\dot{w}_1'(L,t)\dot{u}_1'(L,t)\right),$$
$$V_3 = 0,$$

where $J = (m/3)(C_M^2 + h_M^2) + m(C_M^2 + r_M^2)$, and non conservative work W_{nc} done by the PZT is modeled as

$$W_{nc} = \sum_{s=1}^{2}\int_0^L M_p(t)\Lambda(x_s)w_s''dx_s. \tag{2}$$

$M_p(t)$ is a bending moment produced by PZT due to applied voltage, and $\Lambda(x_s)$ is a distribution function, which defines the location and direction of the bending

moment as shown in Fig. 3(b), and is defined by the heaviside step function $h(x_s - x_0)$ as follows:

$$\Lambda(x_s) = h(x_s - L/2) - h(x_s - 0) - [h(x_s - L) - h(x_s - L/2)]. \quad (3)$$

By using extended Hamilton's principle, which is shown in Eq.(4), the governing equations and the boundary conditions are derived as Eqs. (5) and (6)

$$\delta \int_0^{t_1} \left[\sum_{s=1}^{3} (T_s - V_s) + W_{nc} \right] dt = 0, \quad (4)$$

$$\rho A \ddot{u}_s - EAu_s'' = 0, \ \rho A \ddot{w}_s + EIw_s'''' = M_p(t)\Lambda''(x_s), \quad (5)$$

At $x_s = 0$, (6)

$$u_s = w_s = w_s' = 0,$$

At $x_s = L$,

$$w_1 - w_2 = 0, \ w_1' - w_2' = 0,$$

$$EA\varepsilon_1 + EA\varepsilon_2 + m\ddot{u}_1 - mr_M\ddot{w}_1' = 0, \ EIw_1'' + EIw_2'' - m\ddot{w}_1 - mC_M\ddot{w}_1' = 0$$

$$EIw_1''' + EIw_2''' \quad 2r_M EAu_2' + J\ddot{w}_{12}' + mC_M\ddot{w}_1 \quad mr_M\ddot{u}_1 = 0.$$

In this system, symmetric modes(shown in Fig. (6), which have no influence on the displacement of translational direction at the tip, are negligible. Therefore, as ignoring symmetric modes, $w_1(x,t)$ is assumed to be equal to $w_2(x,t)$ at $0 \le x \le L$.

By using Galerkin's mode summation method, displacement of flexible beam $u_s(x,t)$ and $w_s(x,t)$ are defined as follows:

$$u_s(x,t) = \sum_{i=1}^{n} U_{s,i}(x) q_i(t), \ (s = 1,2), \quad (7)$$

$$w_1(x,t) = w_2(x,t) = \sum_{i=1}^{n} W_i(x) q_i(t), \ (s = 1,2),$$

where $U_{s,i}$ and W_i are mode shape functions of longitudinal and translational direction modes, respectively, $q_i(t)$ is a generalized coordinate. By multiplying the governing equations and boundary conditions by the mode shape functions $U_{s,k}, W_k$ and integrating over the domain, the differential equations satisfying orthogonality condition $(case\ i = k)$ can be obtained as follow: [5]

$$I_i\ddot{q}(t) + K_i q(t) = 2M_p(t) \int_0^L \Lambda''(x) W_k(x) dx \quad (8)$$

$$= 2M_p(t)\left[2W_i'(L/2) - W_i'(L)\right],$$

$$I_i = \rho A \int_0^L U_{1,i}(x)U_{1,j}(x)dx + \rho A \int_0^L U_{2,i}(x)U_{2,j}(x)dx + 2\rho A \int_0^L W_i(x)W_i(x)dx$$

$$+ mU_{1,i}(L)U_{1,j}(L) - mr_M\left[U_{1,i}(L)W_i(L) + U_{1,i}(L)W_i(L)\right] + mW_i(L)W_i(L)$$

$$+ mC_M\left[W_i(L)W_i(L) + W_i(L)W_i(L)\right] + JW_i(L)W_i(L),$$

$$K_i = EA \int_0^L U_{1,i}'(x)U_{1,i}'(x)'dx + EA \int_0^L U_{2,i}'(x)U_{2,i}'(x)dx + 2EI \int_0^L W_i''(x)W_i''(x)dx$$

Eigen functions of uniform beam, which are used for mode shape functions $W_i, U_{s,i}$, are expressed as follows:

$$W_i(x) = [\cos(\sigma_i x) \ \cosh(\sigma_i x) + \lambda_i \{\sin(\sigma_i x) \ \sinh(\sigma_i x)\}]D_i, \quad (9)$$

$$U_{1,i}(x,t) = H_{1,i}\sin\alpha_i L, \ U_{2,i}(x,t) = H_{2,i}\sin\alpha_i L, \quad (10)$$

where $\alpha_i^2 = \rho\omega_i^2 / E, \sigma_i^4 = \rho\omega_i^2 A / EI$, and $\lambda_i, H_{1,i}$ and $H_{2,i}$ can be obtained by using boundary conditions.

$$\lambda_i = \frac{m\sigma_i^3(\cos\sigma_i L - \cosh\sigma_i L) - m\alpha_i^2\sigma_i(\sin\sigma_i L + \sinh\sigma_i L) + 2EI\sigma_i^3(\sin\sigma_i L - \sinh\sigma_i L)}{m\sigma_i^3(\sin\sigma_i L - \sinh\sigma_i L) + m\alpha_i^2\sigma_i(\cos\sigma_i L - \cosh\sigma_i L) - 2EI\sigma_i^3(\cos\sigma_i L + \cosh\sigma_i L)} D_i \quad (11)$$

$$H_{1,i} = \frac{\left[EA2r\left(\frac{\cos\alpha_i L}{\sin\alpha_i L}\right)\alpha_i - \omega_n^2 mr\right]W_i'(L)}{2EA\alpha_i\cos\alpha_i L - \omega_i^2 m\sin\alpha_i L}, \quad (12)$$

$$H_{2,i} = -\frac{2r_1 W_i'(L)}{\sin\alpha_i L} + \frac{\left[2EAr\frac{\cos\alpha_i L}{\sin\alpha_i L}\alpha_i - \omega_i^2 mr\right]W_i'(L)}{2EA\alpha_i\cos\alpha_i L - \omega_i^2 m\sin\alpha_i L}$$

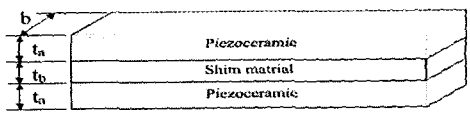

Fig. 4. Layer structure of used bimorph PZT

Fig. 4 shows layer structure of the used bimorph PZT. It is composed of piezoceramics and shim material in center. Because each piezoceramic layer polarized oppositely, bimorph PZT can generate relatively large displacement. We assume that there is a linear relationship between the bending moment $M_p(t)$ generated by the PZT and the applied voltage as follows: [6]

$$M_p(t) = K_p u(t), \ K_p = -d_{31}\left(\frac{t_b + 2t_a}{2}\right)\left(\frac{E_b E_a t_b b}{E_b t_b + 2E_a t_a}\right) \ (s = 1,2), \quad (13)$$

where t_a and E_a are thickness and elastic modulus of piezoceramic, respectively, t_b and E_b are thickness and elastic modulus of shim material, rectively. d_{31} and b are strain constant and width of piezoceramic, respectively. By using proportional structural damping, differential equation of i th mode in Eq.(8) can be reproduced as

$$\ddot{q}_i(t) + 2\zeta_i\omega_i\dot{q}_i(t) + \omega_i^2 q_i(t) = \frac{K_p u(t)}{I_i}\left[4W_i'(L/2) \quad 2W_i'(L)\right]. \quad (14)$$

A reduced dynamic model is represented in state space equation as follow:

$$\dot{\mathbf{X}} = \mathbf{AX} + \mathbf{B}u(t), y_{tip} = w_s(L,t) = \mathbf{CX}, \quad (15)$$

where $\mathbf{X} = [q_1(t)\ \dot{q}_1(t) q_2(t)\ \dot{q}_2(t) \ldots q_n(t)\ \dot{q}_n(t)]^T$,

$$\mathbf{A}=\begin{bmatrix} 0 & 1 & & & \\ -\omega_1^2 & -2\zeta_1\omega_1 & & & \\ & & \ddots & & \\ & & & 0 & 1 \\ & & & -\omega_n^2 & -2\zeta_n\omega_n \end{bmatrix},\quad \mathbf{B}=\begin{bmatrix} 0 \\ \frac{K_p}{I_t}\left[4W_1'(L/2)-2W_1'(L)\right] \\ \vdots \\ 0 \\ \frac{K_p}{I_a}\left[4W_n'(L/2)-2W_n'(L)\right] \end{bmatrix},$$

$$\mathbf{C}=\left[W_1(L)\ \ 0\ \ \cdots\ \ W_n(L)\ \ 0\right].$$

Table. 1. Properties of used bimorph PZT (PIEZO SYSTEM INC,T226-H4SS).

	Piezoceramic	Shim(Stainless steel)
Density (kg/m^3)	7700	7200
Young's modulus (N/m^2)	6.1×10^{10}	
Thickness (mm)	0.27	0.12
Width (mm)	2	2
Length (mm)	16	16
Strain Coefficient (m/V)	-320×10^{-12}	

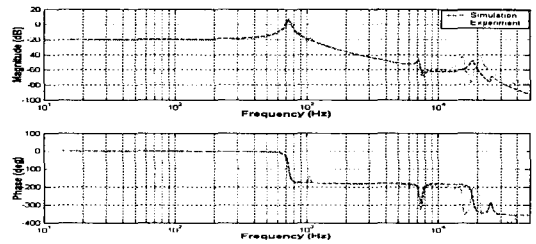

Fig. 5. Frequency responses of PZT Actuator.

Modeled mode			Unmodeled mode	
1st Translational mode : 703.42 Hz	2nd Translational mode : 7821 Hz	3rd Translational mode : 14360 Hz	Symmetric mode : 7975 Hz	Vertical mode : 997.12 Hz

Fig. 6. Natural frequencies and mode shapes obtained by FE Analysis.

Dimensions and mechanical specifications of the bimorph PZT are shown in Table 1. Fig. 5 shows the frequency responses of PZT actuator. The solid line and broken line represent experimental and simulational result, respectively. In experiment, LDV(Laser Doppler Vibrometer, Polytech OFV3001) is used for sensing the displacement of tip mass and DSA(Digital Signal Analyzer, HP 35670A) is used for analyzing the signal. The simulational results obtained from the dynamic model in Eq. (15) agree well with the experimental results in lower frequency range and a few modeling uncertainties can be reduced by proper design of robust controller, which is described later. And, the effect of the modeling uncertainties in higher frequency range is negligible, because the bandwidth of the control system is restricted to low frequency range. Fig. 6 shows natural frequencies and mode shapes obtained by FE analysis, and these frequencies coincide with simulational results.

4. Sliding mode control

There are various modeling uncertainties in this actuator system due to the nonlinearity in PZT, measurement error, and modeling inaccuracies. These modeling uncertainties can be represented as parameter variations in damping constants, natural frequencies, and bending moment generated by the actuator as follows:

$$\underline{\omega_i}=\omega_i+\delta\omega_i,\quad \frac{|\delta\omega_i|}{\omega_i}\le\beta_i, \tag{16}$$

$$\underline{\zeta_i}=\zeta_i+\delta\zeta_i,\quad \frac{|\delta\zeta_i|}{\zeta_i}\le\gamma_i,$$

$$M_p(t)=(K_p+\delta K_p)u(t)\quad ,\frac{|\delta K_p|}{K_p}\le\alpha, \tag{17}$$

where $\underline{\omega_i}$ and ω_i are natural frequency and its nominal value, respectively, and $\underline{\zeta_i}$ and ζ_i are damping ratio and its nominal value, respectively. $\delta\omega_i$ and $\delta\zeta_i$ are bounded parameter variations in $\underline{\omega_i}$ and $\underline{\zeta_i}$, respectively, and β_i and γ_i are their bounds. And δK_p is variable but bounded by weighting factor α.

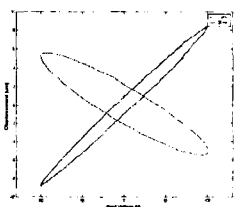

Fig. 7. Hysteresis Loop (25Hz & 1KHz).

Fig. 7 shows the hysteresis loop of the PZT actuator employed in this work, and from this figure, the weighting factor α in Eq. (17) is determined as 0.13. The state equation and output equation are obtained from Eqs from (15) to (17) as follows:

$$\dot{\mathbf{X}}=(\mathbf{A}+\delta\mathbf{A})\mathbf{X}+(\mathbf{B}+\delta\mathbf{B})u(t), \tag{18}$$

$$y_{tip}=\mathbf{C}\mathbf{X},$$

where,

$$\delta\mathbf{A}=\begin{bmatrix} 0 & 0 & & & \\ -2\omega_1\delta\omega_1-\delta\omega_1^2 & -2\zeta_1\delta\omega_1 & & & \\ & & \ddots & & \\ & & & 0 & 0 \\ & & & -2\omega_n\delta\omega_n-\delta\omega_n^2 & -2\zeta_n\delta\omega_n \end{bmatrix},\quad \delta\mathbf{B}=\begin{bmatrix} 0 \\ \frac{\delta K_p}{I_t}\left[4W_1'(L/2)-2W_1'(L)\right] \\ \vdots \\ 0 \\ \frac{\delta K_p}{I_a}\left[4W_n'(L/2)-2W_n'(L)\right] \end{bmatrix}.$$

$\mathbf{A}$ and $\mathbf{B}$ are nominal part of the system and input matices, respectively, and $\delta\mathbf{A}$ and $\delta\mathbf{B}$ are their uncertainty parts.

We apply the sliding mode control algorithm in order to make the system to be robust against the modeling uncertainties. A sliding surface which guarantees stable

sliding mode motion on the surface itself, is expressed as follows:

$$S=\dot{\tilde{y}}+\lambda\tilde{y}=\left[\sum_{i=1}^{n}W_i(L)\dot{q}_i(t)-\dot{y}_d\right]+\lambda\left[\sum_{i=1}^{n}W_i(L)q_i(t)-y_d\right], \quad (19)$$

where, λ is a positive constant and $\tilde{y}$ is a tracking error, y_d is desired trajectory of the tip of the PZT actuator. Then, the Sliding mode condition, which guarantee that the state variables of the system during the sliding mode motion are constrained to the surface, is expressed as follows:

$$S\dot{S}\le 0. \quad (20)$$

Then, sliding mode controller which satisfies the sliding mode condition can be obtained as shown in Eq. (21). [7]

$$u(t)=\frac{1}{K_p P}\left\{\lambda\left[\sum_{i=1}^{n}W_i(L)\dot{q}_i(t)-\dot{y}_d\right]+\left[\sum_{i=1}^{n}W_i(L)\left(r_{2i-1}q_i(t)+r_{2i}\dot{q}_i(t)\right)-\ddot{y}_d\right]+k(\mathbf{X})sat\left(\frac{S}{\Phi}\right)\right\}, \quad (21)$$

$$P=\sum_{i=1}^{n}\frac{W_i(L)}{I_i}\left[4W_i'(L/2)-2W_i'(L)\right],$$

where, $k(\mathbf{X})\ge\left[\sum_{i=1}^{n}|W_i(L)|d+\sum_{i=1}^{n}|W_i(L)|\left(|z_{2i-1}q_i(t)|+|z_{2i}\dot{q}_i(t)|\right)\right]$,

$$z_{2i-1}=-(2\beta+\beta^2)\omega_i^2, \qquad r_{2i-1}=-\omega_i^2,$$

$$z_{2i}=-2\zeta_i(\beta+\gamma+\beta\gamma)\omega_i, \quad r_{2i}=-2\zeta_i\omega_i,$$

$$d=K_p\alpha Pu(t).$$

Φ is thickness of boundary layer and the saturation function is used to decrease the chattering in control input. The first flexible mode of the PZT actuator is considered in designing the controller, because there should be a limitation in control bandwidth due to the modeling uncertainties in higher frequency range. In order to reduce the spillover effect due to the higher modes, λ must be chosen to be small enough with respect to the frequencies of those modes.

5. Linear observer

In this work, we use a linear observer to estimate the entire elements of state vector $\mathbf{X}_e(t)=\left[\hat{q}_1(t)\ \dot{\hat{q}}_1(t)\ldots\hat{q}_n(t)\ \dot{\hat{q}}_n(t)\right]^T$. Conventional observer can be expressed as follows:

$$\dot{\mathbf{X}}_e(t)=(\mathbf{A}-\mathbf{LC})\mathbf{X}_e(\mathbf{t})+\mathbf{B}u+\mathbf{L}y(t), \quad (22)$$

where $\mathbf{L}$ is observer gain matrix. And the sliding mode controller using the observer is expressed as follows:

$$u(t)=\frac{1}{K_p P}\left\{\lambda\left[\sum_{i=1}^{n}W_i(L)\dot{\hat{q}}_i(t)-\dot{y}_d\right]+\left[\sum_{i=1}^{n}W_i(L)\left(r_{2i-1}\hat{q}_i(t)+r_{2i}\dot{\hat{q}}_i(t)\right)-\ddot{y}_d\right]+k(\mathbf{X}_e)sat\left(\frac{S_e}{\Phi}\right)\right\} \quad (23)$$

where, $k(\mathbf{X}_e)\ge\left[\sum_{i=1}^{n}|W_i(L)|d+\sum_{i=1}^{n}|W_i(L)|\left(|z_{2i-1}q_i(t)|+|z_{2i}\dot{q}_i(t)|\right)\right]$.

The sliding surface is represented as $S_e=0$ instead of $S=0$, and S_e is obtained by replacing the state vector $\mathbf{X}$ by its observed state vector $\mathbf{X}_e$ in the expression of S. As we use linear observer in order to observe the state in nonlinear system, observation error can be arisen. However, if $k(\mathbf{X}_e)$ is chosen to be large enough to compensate both modeling uncertainties and linear observer inaccuracies, the sliding mode controller can yield $S_e\to 0$ as $t\to\infty$. And, if the states in the observer converge to the actual states despite the modeling uncertainties, S_e converges to S. Therefore, the actual states converges to desired states as $S\to 0$.[8] Fig. 8 shows the Block diagram of sliding mode control system with linear observer.

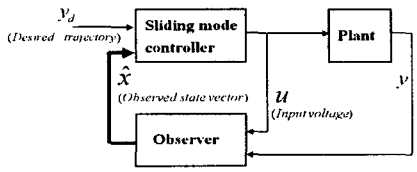

Fig. 8. Block diagram of sliding mode control system with linear observer

6. Experimental result

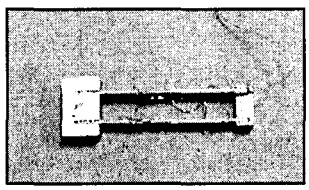

Fig. 9. Photograph of PZT actuator

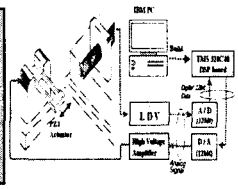

Fig. 10. Experimental setup

Fig. 9 shows the photograph of the proposed PZT actuator, and Fig. 10 shows simple diagram of experimental setup. A DSP based control system is used to implement sliding mode controller with observer, LDV is used to measure the displacement of the tip mass. Control voltage computed by sliding mode controller, excites PZT actuator through precise 12bit DA converter and high voltage amplifier. PZT actuator is mainly charged to track the RO(Run Out) harmonic which is risen from disc media. Although the RO harmonic is difficult to be measured, DVD specification book explains that the main RO harmonic is risen in 25Hz in case of 1×speed DVD. Therefore we choose the desired trajectory to 25Hz single sinusoidal trajectory, and Fig. 11(a) shows the result of the experiment. In practice, RO harmonic is shown as combination of sub RO harmonics which are assumed to be risen in multiple frequencies (such as 50Hz, 75Hz, 100Hz……). Therefore, we choose the desired trajectory as the combination of 25Hz and 100Hz sinusoidal trajectories.

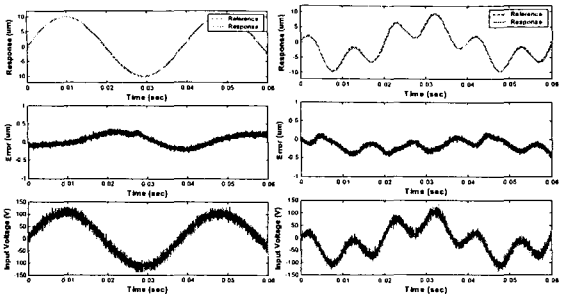

(a) (b)

Fig. 11. Tracking responses of PZT actuator:

(a) $y_d = 10\sin(2\pi \times 25 \times t)$,

(b) $y_d = 6\sin(2\pi \times 25 \times t) - 4\sin(2\pi \times 100 \times t)$.

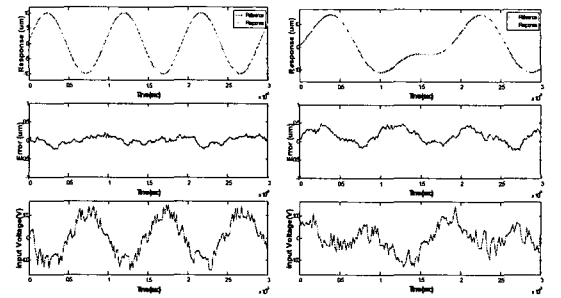

(a) (b)

Fig. 12. Tracking responses of PZT actuator:

(a) $y_d = 10\sin(2\pi \times 1000 \times t)$,

(b) $y_d = 10\sin(2\pi \times 10^3 \times t) + 5\sin(2\pi \times 500 \times t)$

Fig. 11(b) shows the experimental result, and each result shows 4 to 5% error rates. It is clearly observed that tracking performances fairly good. Fig. 12(a) and Fig. 12(b) show the tracking response for 1KHz single sinusoidal trajectory and combination of 500Hz and 1KHz sinusoidal trajectories, respectively. Each result shows $0.25\mu m(2.5\%)$, $0.5\mu m$ (3%) error. It is also seen that actual trajectory follow well to the high frequency desired trajectories in spite of large amount of hysteric behavior in PZT actuator as shown in Fig. 7. Fig. 13 shows the response for 10 μm step trajectory. It is clearly observed that actual states fast converge to the desired states.

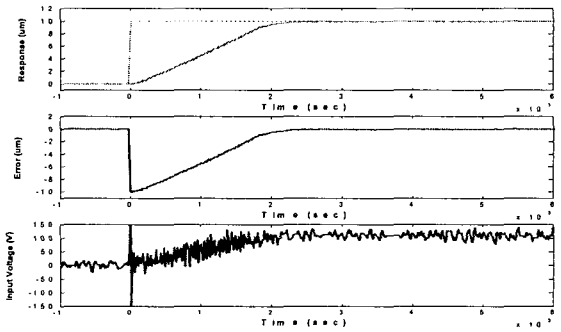

Fig. 13. Step response of PZT actuator.

7. Conclusion

In this work, we proposed the swing-arm type dual-stage actuator for SFF ODD that is suitable for fast seeking and precise track following control. The dynamic model of the PZT actuator was derived by using the Hamilton's principle, and verified by comparing with the experimental frequency response. The sliding mode control with observer was designed for the system to be robust against the modeling uncertainties including the nonlinearity in PZT, measurement error, and modeling inaccuracies. The simulations and the experimental results showed that the proposed sliding mode control scheme produced good tracking following performances and guarantees the stability robustness against various uncertainties.

Acknowledgement

This work supported by the Korea Science and Engineering Foundation(KOSEF) through the CISD at Yonsei university under grant No.2000G0102.

Reference

(1) Mori K, Munemoto T, Otsuki H, Yamaguchi Y, Akagi K, 1991, "A dual-stage magnetic disk drive actuator using a piezoelectric device for a high track density", IEEE Transe. Magnetics., Vol. 27, No. 6, pp. 5298~5300.

(2) Evans RB, Griesbach, JS, 1999, "Piezoelectric microactuator for dual stage control", IEEE Transe. Magnetics., Vol. 35, No. 2, pp. 977-982.

(3) Guo L, Martin D, Brunnett D, 1999, "Dual-stage actuator servo control for high density disk drives", IEEE/ASME International Conference on Advanced Intelligent Mechatronics, pp. 132-137.

(4) Won-Ik Cho, No-Cheol Park, Hyun-Seok, Young-Pil Park, 2002, "Swing-arm-type PZT dual actuator with fast seeking for optical disk drive", Microsystems Technologies, Vol. 8, pp. 139~148

(5) Anderson GL, 1978, "Natural frequency of two cantilever joined by a rigid connector at their free ends", J Sound Vibration, Vol. 57, No. 3, pp. 403~412

(6) Bailey T, Hubbard Jr JE. 1985, "Distributed piezoelectric-polymer active vibration control of a cantilever beam.J Guidance", Control and Dynamics, Vol. 8, No. 5, pp. 605-611

(7) S.B.Choi, H.K.Kim, S.C.Lim, Y.P.Park, 2001, "Position tracking control of an optical pick-up device using piezoceramic actuator", J Mechatronics, Vol. 11, pp. 691-705

(8) Jean-Jacques E.Slotine, Weiping Li, Applied Nonlinear Control, Prentice-Hall